REPORT DOCUMENTATION PAGE						Form Approved OMB No. 0704-0188

The public reporting burden for this collection of information is estimated to average 1 hour per response, including the time for reviewing instructions, searching existing data sources, gathering and maintaining the data needed, and completing and reviewing the collection of information. Send comments regarding this burden estimate or any other aspect of this collection of information, including suggestions for reducing the burden, to Department of Defense, Washington Headquarters Services, Directorate for Information Operations and Reports (0704-0188), 1215 Jefferson Davis Highway, Suite 1204, Arlington, VA 22202-4302. Respondents should be aware that notwithstanding any other provision of law, no person shall be subject to any penalty for failing to comply with a collection of information if it does not display a currently valid OMB control number.
PLEASE DO NOT RETURN YOUR FORM TO THE ABOVE ADDRESS.

Field	Value
1. REPORT DATE *(DD-MM-YYYY)*	28-09-2005
2. REPORT TYPE	Final Report
3. DATES COVERED *(From - To)*	01 Oct 02 - 30 Jun 05
4. TITLE AND SUBTITLE	Intersublevel Infrared Detectors
5a. CONTRACT NUMBER	
5b. GRANT NUMBER	DAAD19-02-1-0437
5c. PROGRAM ELEMENT NUMBER	
5d. PROJECT NUMBER	
5e. TASK NUMBER	
5f. WORK UNIT NUMBER	
6. AUTHOR(S)	D. Pal and E. Towe (PI)
7. PERFORMING ORGANIZATION NAME(S) AND ADDRESS(ES)	Carnegie Mellon University 5000 Forbes Avenue Pittsburgh, PA 15213
8. PERFORMING ORGANIZATION REPORT NUMBER	CMU-Towe-2005.09.30
9. SPONSORING/MONITORING AGENCY NAME(S) AND ADDRESS(ES)	US Army Research Office 4300 S. Miami Boulevard Durham, NC 27703-9142
10. SPONSOR/MONITOR'S ACRONYM(S)	AMSRD-ARL-RO-EL
11. SPONSOR/MONITOR'S REPORT NUMBER(S)	44277.1-EL
12. DISTRIBUTION/AVAILABILITY STATEMENT	Public Distribution / Availability Unlimited
13. SUPPLEMENTARY NOTES	N/A

14. ABSTRACT

This is the Final Report of ARO Grant No. DAAD19-02-1-0437. It is a report on the characteristics of (InGa)As/GaAs long-wave (8 - 12 μm) quantum-dot infrared photodetector structures. Peak responsivities and detectivities were measured using a calibrated black body source. The results of this work indicate that for the structures characterized here, the maximum operating temperature is limited to 105 K. No effort was made in the original design of the device structure for higher temperature operation. For operation at temperatures higher than this, one must investigate other device structures; such structures have been identified and will be the subject of future work. The work reported here has paved the way to the identification of candidate device structures for high operating temperature (HOT) quantum-dot detector

15. SUBJECT TERMS

Quantum Dots, Infrared Detectors, Night Vision;

16. SECURITY CLASSIFICATION OF: a. REPORT	b. ABSTRACT	c. THIS PAGE	17. LIMITATION OF ABSTRACT	18. NUMBER OF PAGES	19a. NAME OF RESPONSIBLE PERSON	19b. TELEPHONE NUMBER *(Include area code)*
U	U	U	UU	11	Elias Towe	412-268-2860

Standard Form 298 (Rev. 8/98)
Prescribed by ANSI Std. Z39.18

Final Report

on

Long-wave (8 – 12 μm) Quantum-dot Infrared Photodetectors

D. Pal and E. Towe (PI)

Laboratory for Photonics
Carnegie Mellon University
Pittsburgh, PA 15213

Work performed under ARO Grant DAAD19-02-1-0437

Monitored by Dr. William Clark

Reporting Period: July 1, 2004 – June 30, 2005

Executive Summary

This is the Final Report of ARO Grant No. DAAD19-02-1-0437. It is a report on the characteristics of (InGa)As/GaAs long-wave (8 - 12 μm) quantum-dot infrared photodetector structures. Peak responsivities and detectivities were measured using a calibrated black body source. The results of this work indicate that for the structures characterized here, the maximum operating temperature is limited to 105 K. No effort was made in the original design of the device structure for higher temperature operation. For operation at temperatures higher than this, one must investigate other device structures; such structures have been identified and will be the subject of future work. The work reported here has paved the way to the identification of candidate device structures for high operating temperature (HOT) quantum-dot detectors.

1.0 Introduction

This document is the Final Report of our research on long-wave (8 – 12 μm) infrared quantum-dot photodetectors fabricated from the (In,Ga)As/GaAs materials system. This work was supported under ARO Grant Number DAAD19-02-1-0437. The major goal during the past year was to carry out a careful and detailed study of some of the main characteristics of these devices. This study was intended to point the way toward improving and optimizing the device characteristics such as peak responsivity, detectivity, and photoconductive gain. The implicit long-term objective of the work was to pave the way toward high operating temperature (HOT) focal plane imagers.

2.0 Device Structures

The InGaAs/GaAs quantum-dot structures were grown by a solid-source molecular beam epitaxy techniques on semi-insulating GaAs substrates. A typical structure consists of five periods of InGaAs/GaAs quantum dots sandwiched between two heavily doped GaAs layers. The thickness of the GaAs barrier in the InGaAs/GaAs superlattice is about 50 nm. The dots are doped with silicon to supply about two electrons per dot. And atomic force microscopy (AFM) was used to study the surface distribution of dots; these observations were carried out on an uncapped InGaAs layer of the dots. From these observations, we estimate that the lateral extent of a dot is about 20 nm, while its average height is about 6 nm. The areal dot density was estimated to be between 6.0 and 6.8 x 10^{10} cm^{-2}.

3.0 Device Characteristics

In order to study the device characteristics of the quantum dots, we fabricated devices of different sizes using conventional photolithography and wet chemical etching.

The top and bottom ohmic contacts were fabricated by annealing n-type Ni/AuGe/Au contacts. The front side of the structures was then illuminated with normally incident black body radiation to explore the spectral characteristics. Dark current-voltage characteristics were measured at various temperatures using a semiconductor parameter analyzer.

3.1 Dark Current

In these detectors, dark current originates from different sources: these are (a) thermoionic, (b) thermally assisted tunneling, and (c) temperature-independent tunneling. In the thermoionic process, carriers from dots are thermally excited to continuum states and from there contribute to the dark current. The current due to thermoionic emission processes increases exponentially with temperature. Thermoionic processes generally dominate above 50 K. In the thermally assisted tunneling process, carriers are thermally excited into higher energy levels within a dot, but just below the top of the conduction band edge; they then tunnel through the triangular tip of the barrier into states on the other side of the barrier that

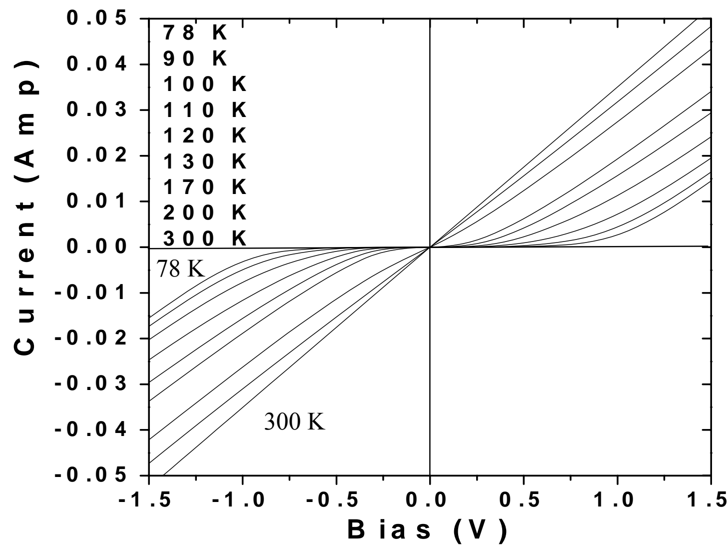

Fig. 1(a): Current-voltage characteristics of a QDIP (in the dark) on a linear scale plot.

support conduction. Finally, there is temperature-independent tunneling current; this is due to tunneling of carriers between dots or between the dots and the wetting layers.

In Fig. 1, we show the variation of the dark current as a function of temperature in both linear and log scale; the linear dependence is shown in Fig. 1(a); Fig. 1(b) shows the same data on a semi-log plot. In the linear plot, the current-voltage characteristics of the device go from rectifying to ohmic as the temperature is increased from 78 to 300 K. There is a distinct transition temperature around 170 K. At the bias voltage of 0.25 V, the dark current decreases by three orders of magnitude as the temperature is lowered from 300 to 78 K; this is probably due to carrier freeze-out in the dots. Electrons are trapped in states within the dots as the temperature is lowered from 300 to 78 K. When this happens, the number of free electrons that would ordinarily contribute to conduction is decreased; in other words, there is depletion and the device acts as a rectifier. As the temperature is raised, the trapped electrons are re-emitted into conduction states by thermal energy. The rectifying structure then turns into an ohmic conductor. Fig. 1 (b) shows the current- voltage characteristics on a semi-

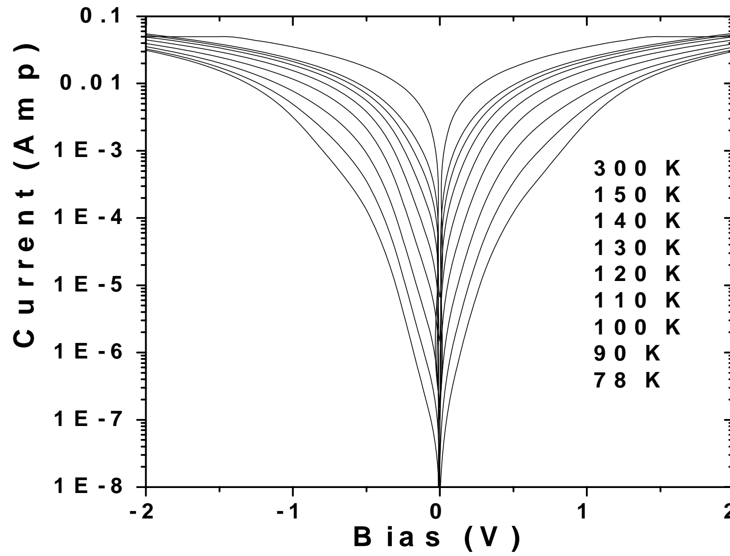

Fig. 1(b): Current-voltage characteristics of a QDIP (in the dark) on a logarithmic scale.

logarithmic plot. It is difficult to observe and identify the change of the device characteristics from rectifying to ohmic in this case.

In order to study the thermally activated processes in the device structures, we have constructed Arrhenius plots of the dark current for a fixed bias voltage point, but for varying temperatures. One such plot is shown in Figs. 2 (a) for selected positive biases; a similar plot can be obtained for selected negative biases. By considering only the linear portions of the plots, we have been able to extract the activation energies for the thermal processes involved. The activation energy variation as a function of bias voltage is shown in Fig. 3. It is found that the activation energy decreases from 155 meV to 20 meV when the bias voltage is raised from 0.02 to 1.4 V. Note the symmetry of the activation energy plot as a function of positive and negative bias voltages; this is a direct consequence of the symmetry of the device structure.

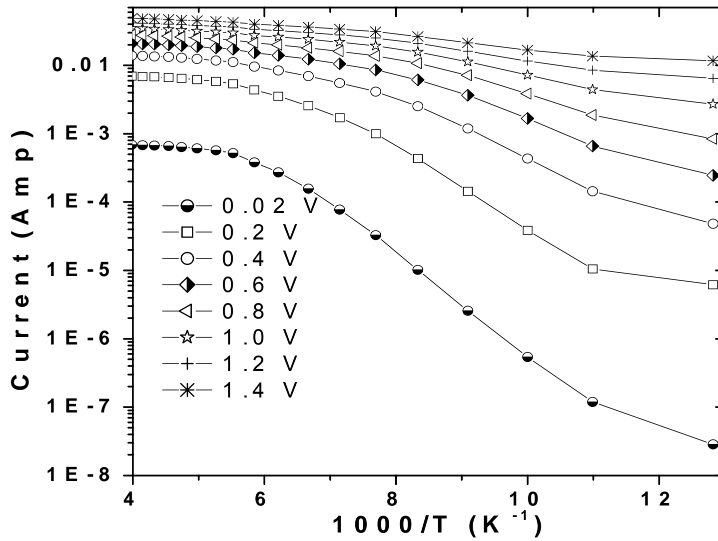

Fig. 2(a): Arrhenius plot of the dark current under positive bias

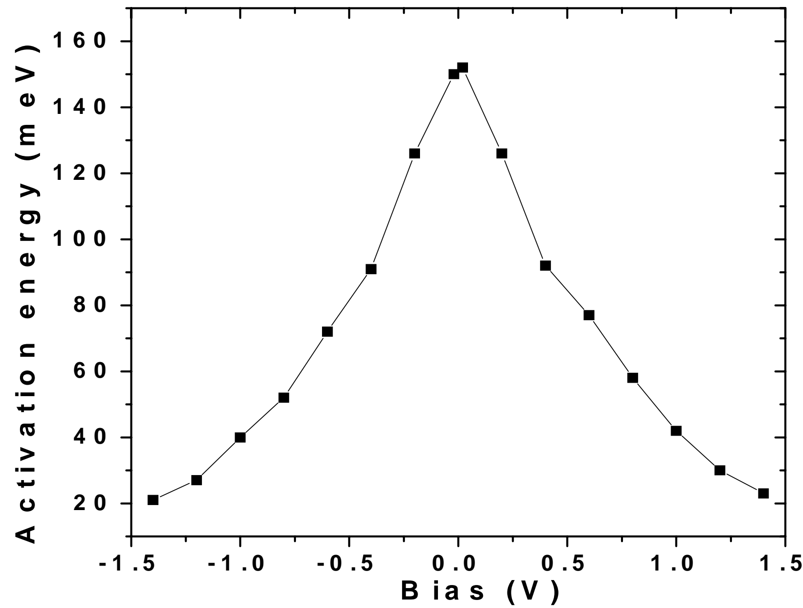

Fig. 3: Activation energy as a function of bias voltage.

3.2 Spectral Characteristics

The interband emission characteristics of the dots are studied by using photoluminescence spectroscopy at 78 K. The luminescence emission peak was observed at 1.18 eV, with a spectral width of the emission being about 28 meV. This narrow line-width indicates that the quantum dots are of fairly uniform size. For inter-sublevel characteristics, we use a Fourier Transform Infrared Spectrometer with a broadband black body (1 – 20 μm) source. Figure 4 shows the normal-incidence photoresponse at different bias voltages. The incident light used in this experiment is unpolarized and the measurement was performed at 78 K. Note that one observes a single absorption peak located at about 10.1 μm. There is also a broad secondary shoulder located at about 7.5 to 9.5 μm. The full-width-at-half-maximum intensity of the absorption spectrum is about

1.14 μm; the quantity Δλ/λ is about 11.3 %. This is a measure of the absorption line-width; the narrowness of the line-width is generally a reflection of the uniformity of the dots. Furthermore, one can infer that the transitions involved in this absorption from a lower bound state to a higher bound state. The peak observed at 10.1 μm is probably due to a transition from the ground states (E_0) to the first excited state (E_1). Note that the peak absorption wavelength remains relatively unchanged at different positive and negative bias voltages. Furthermore, no appreciable change in cut-off wavelength in the photoresponse is observed with increasing bias voltage. This confirms that the transition related to the peak at 10.1 μm is from bound states within the dots. The broad shoulder around 7.5 to 9.5 μm is probably from a transition between the ground state and the second excited state or a state in the continuum.

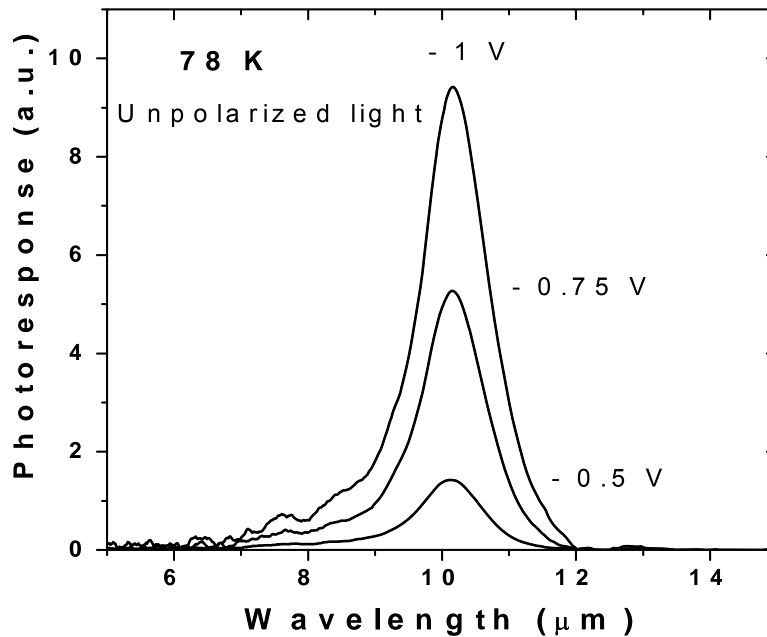

Fig. 4: Relative spectral response at different bias voltages.

Figure 5 shows the photo-response at three different temperatures: 78, 95 and 105 K in the normal incidence mode. It is evident that the intensity decreases as the

temperature is raised. One possible explanation is that as the temperature is raised, more free electrons become available to occupy the higher energy states in the dots; as a consequence, the population of empty states that would be available for optical absorption transitions is decreased, leading to a decrease in the intensity of the absorption. Since photoconductivity is proportional to mobility and carrier lifetime, the decrease in the photo-excited carrier lifetime at higher temperatures may also contribute to the lower photo-response. While there is a notable decrease in absorption with temperature, there is no change in the peak wavelength of absorption from 78 to 105 K. The energy band gaps of GaAs and InGaAs generally shrink with increasing temperature; as a consequence, the electronic energy states in a quantum dot move to lower energy values as the temperature is increased. However, the separation between the energy levels remains the same. This is borne out in the observed photo-response spectra at different temperatures.

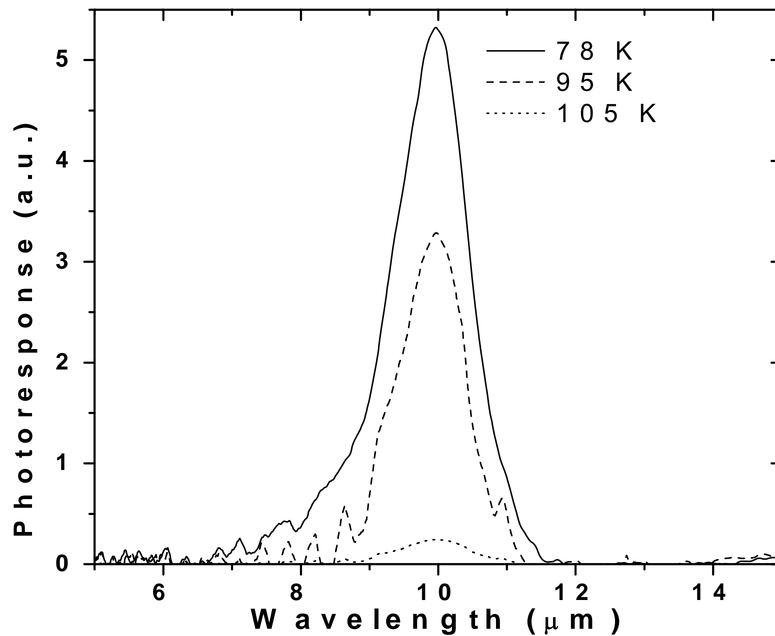

Fig. 5: Relative spectral response at different temperatures.

3.3 Responsivity

We have measured the spectral responsivity of the devices studied in this work; the absolute responsivity was calibrated using a standard blackbody source. The noise of the blackbody response is measured at different temperatures and bias voltages. For the calibration, the temperature of the blackbody source was maintained at 500°C. Germanium was used as a filter to obtain the signal due to the quantum dots. The quantum-dot photocurrent signal and the noise were measured using a Keithley Model 428 current amplifier and a Stanford Research Model SRS 760 network analyzer; this analyzer displays the fast Fourier Transform (FFT) spectrum of the voltage as a function of frequency. The infrared light from blackbody source was chopped at a frequency of about 507 Hz, which is not a multiple of 60 Hz to distinguish the photocurrent signal from line AC noise. The photocurrent response was measured by averaging the detector signal over a 50-Hz bandwidth, centered around the chopper frequency. The noise voltage was also measured using the

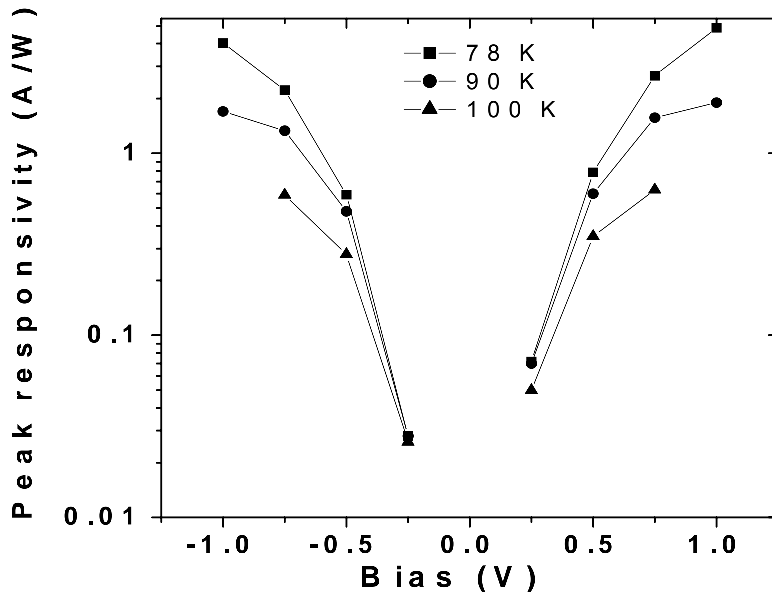

Fig.6: Peak responsivity at 78 K, 90 K, and 100 K.

same bandwidth and chopper frequency (507 Hz), which is in the flat-band region of the FFT spectrum. Figure 6 shows the spectral peak responsivity as a function of bias at different temperatures. The peak responsivity at 78 K increases from 72 mA/W to 4.9 A/W when the bias voltage is raised from 0.25 to 1.0 V. For negative bias, the responsivity increases from 28 mA/W to 4.02 A/W as the bias voltage is changed from –0.25 to –1.0 V. The different responsivity values for the same magnitude of negative and positive bias voltages is probably due to asymmetric shape of the quantum dots along the growth direction, and also because of the wetting layers under the quantum dots. Because of this, electrons in dots encounter different barrier heights—depending on whether transport is toward the top or bottom contacts.

3.4 Detectivity

The peak detectivity, D^*, is a measure of the signal-to-noise ratio and is calculated from the measured noise current and responsivity using the relation:

$D^* = R_p (A\,\Delta f)^{1/2} / i_n$, where R_p, A, Δf, i_n are, respectively, peak responsivity, area of the detector, measurement band width and noise current. The detectivity values

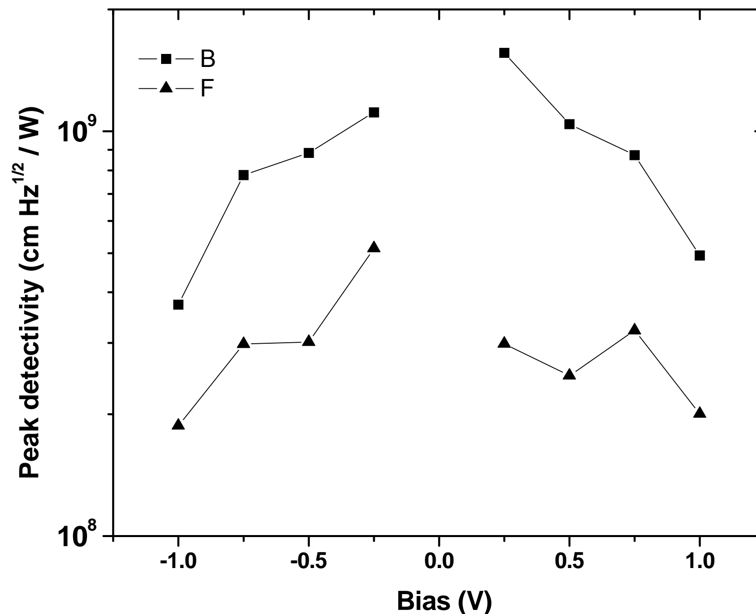

Fig. 7: Peak detectivity at 78 K and 90 K.

for different bias voltages and temperatures are shown in Fig. 7. For the bias voltages of +/- 0.25 V, detectivities are about 1.6 x 10^9 and 1.1 x 10^9 cm $Hz^{1/2}$/W, respectively at 78 K. The detectivity decreases with increasing temperature, as well as bias voltage. It is observed to decrease to 4.9 x 10^8 and 3.7 x 10^8 cm $Hz^{1/2}$/W from 1.6 x 10^9 and 1.1 x 10^9 cm $Hz^{1/2}$/W, when the bias voltage is raised from 0.25 to 1.0V and – 0.25 to – 1.0 V, respectively. With an increase in temperature from 78 to 100 K, the detectivity decreases from 1.6 x 10^9 to 3 x 10^8 cm $Hz^{1/2}$/W at 0.25 V and from 1.6 x 10^9 to 5.2 x 10 ^{8} cm $Hz^{1/2}$/W at – 0.25 V. The decrease of detectivity with an increase in temperature and bias voltage is likely due to an increase in dark current.

4.0 Summary

We have measured a high peak responsivity as high as 4.9 A/W and peak detectivity as high as 1.9 x 10^9 cm $Hz^{1/2}$/W at 78 K. However, the present device design cannot be used for operation beyong 105 K since the responsivity and detectivity decreases with increasing temperature. For operation at temperatures higher than this, one must investigate other structures; this will be the subject of future work. We have several ideas on how to lower the dark current and how toredesign the devices so that they can operate at temperatures beyond 105 K.